16th World Conference on Earthquake, 16WCEE 2017
Santiago Chile, January 9th to 13th 2017
Paper N° 2616
Registration Code: S-T1464293744

Experimental Study on the Response of Fiber Reinforced Elastomeric Isolators Under Combined Loading

Y. Al-Anany[(1)], M.J. Tait[(2)], M. Moustafa[(3)], M. Torrie[(4)]

[(1)] *Ph.D. Candidate, McMaster University, Canada, alananym@mcmaster.ca*
[(2)] *Professor, JNE Consulting Chair in Design, Construction, and Management in Infrastructure Renewal McMaster University, Canada, taitm@mcmaster.ca*
[(3)] *Assistant Professor, Department of Civil and Environmental Engineering, University of Nevada, Reno, mmoustafa@unr.edu*
[(4)] *M.Eng, P.Eng Bridge Engineer, Associated Engineering, Canada, torrie@ae.ca*

Abstract

The objective of seismic isolation is to decouple the superstructure from earthquake induced ground motions. The introduction of properly designed low horizontal stiffness elements between the superstructure and the foundation, which are capable of carrying the vertical loads to the foundation, can significantly reduce the seismic demand and seismic-induced damage. Numerous isolation systems have been developed for this purpose. Fiber reinforced elastomeric isolators (FREI) are a relatively new type of reinforced elastomeric isolator. A unique feature of FREI is that individual isolators of any plan geometry can be rapidly cut from a large pre-manufactured sheet. FREI are typically categorized as either bonded (B-FREI) or unbonded (U-FREI). Early investigations have revealed that U-FREI can effectively protect a structure and its non-structural components from moderate and strong seismic events. Although both the vertical and lateral response of U-FREI have been investigated experimentally, few tests have been carried to evaluate the influence of rotational deformations on the vertical and lateral response of U-FREI. This paper reports on an experimental investigation of the response of U-FREI under combined vertical, lateral and rotational deformations. The experimental program was conducted using a 3 degree-of-freedom test apparatus. Based on findings from the experimental tests, the paper offers recommendations for the design and manufacture of U-FREI.

Keywords: seismic isolation; fiber-reinforced; elastomeric; rotational deformation; bridges application;

1. Introduction

Attention to the seismic design of bridges has significantly increased after a number of bridge failures during major seismic events (e.g. 1971 San Fernando, 1989 Loma Prieta, and 1994 Northridge, California earthquakes, 1995 Kobe, Japan, and 1999 Chi-Chi, Taiwan earthquakes). The observed damage to bridges following these seismic events confirms the importance of proper seismic design **[1]**. Additionally, it was found that employing traditional methods to increase the seismic capacity of a bridge were not as effective as anticipated **[2]**. These observations highlighted the importance of introducing innovative techniques and devices that are effective in mitigating damage. A reduction in the seismic demand on bridge components can be achieved through seismic isolation. This method introduces elements (seismic isolators) with low lateral stiffness between the bridge superstructure (i.e. deck/girders) and substructure (i.e. pier/abutment), as shown in **Fig. 1**.

The main role of seismic isolators is to reduce and redistribute the seismic forces and accelerations imposed on the bridge superstructure and substructure **[3].** However, the isolators must be able to adequately resist and transmit the loads/deformations from the substructure to the superstructure. This requires that the isolators possess sufficient vertical stiffness and are able to accommodate the rotational deformations that can be induced by the bridge superstructure during the lifetime of the bridge **[4]**.

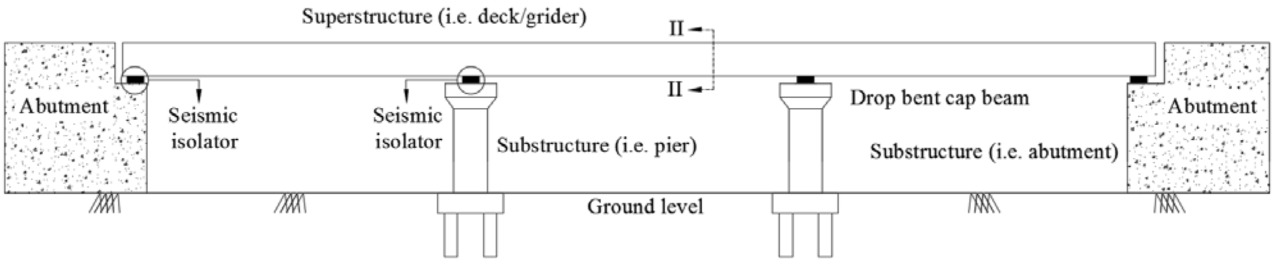

(a)

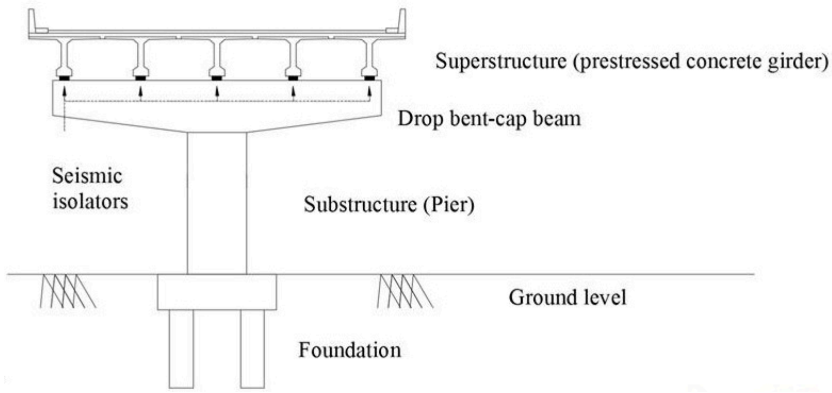

(b)

Fig. 1 – A typical seismically-isolated bridge: (a) elevation; and (b) section II-II

Early investigations revealed that steel reinforced elastomeric bearings/isolators can support/accommodate the aforementioned loads/deformations as well as provide a high level of isolation efficiency **[3]**. However, steel reinforced elastomeric isolators can be heavy and expensive and the reinforcement is vulnerable to corrosion. Thus, bridge design codes, such as CAN/ -S6 Canadian Highway Bridge Design Code (CHBDC) (CSA 2014) **[5]** and the American Association of State Highway and Transportation Officials (AASHTO) LRFD Bridge Design Specifications**) [6,7]** allow the replacement of steel with other type of reinforcement materials. However, the employed reinforcement should not be affected when exposed to water, cold or hot temperatures or other environmental effects, as long as it is capable of withstanding the expected stresses and deformations.

The viability of replacing the steel reinforcement in traditional elastomeric isolators with another material such as carbon fiber fabric has been investigated, both experimentally and analytically, by a number of researchers **[8-13]**. One of the primary objectives of these studies was to confirm the feasibility of using a lighter fiber fabric as the reinforcement material instead of steel. Since the fiber reinforcement possesses negligible flexural rigidity, unlike rigid steel plates, it was observed that unbonded fiber reinforced elastomeric isolators (U-FREI), which are constructed without thick steel end plates and are simply placed unfastened and unbonded between the superstructure and the substructure, undergo a unique rollover behavior under lateral deformation. U-FREI are lightweight due to the elimination of the steel reinforcement and steel end plates. Furthermore, a reduction in cost is expected for FREI because of the reduction in the labor intensity associated with manufacturing relative to that of steel reinforced elastomeric isolators.

The two major factors that are found to influence the response of U-FREI are the shape factor, defined as the ratio of the loaded area to the free bulging area of the elastomer, and the aspect ratio, defined as the ratio of total width/length to height. The shape factor is a parameter that strongly influences the vertical response, while the aspect ratio is the controlling parameter for the stable response of U-FREI under lateral deformation. Even though a number of research studies have been carried out to investigate the vertical and lateral response of U-FREI, few studies to date **[14-16]** have considered the effect of rotational deformations, which can be crucial in the design of bridges. Accordingly, the objective of this paper is to present recent work on the influence of rotational deformations on the vertical and lateral response of U-FREI. Results from experimental testing are presented in Section 2 and models that can be used to simulate the lateral response of U-FREI are presented in Section 3.

2. Experimental Program

2.1 Specimen

A multilayer sheet consisting of elastomer reinforced by layers of carbon fibers fabrics (i.e. FREI) was manufactured in the Applied Dynamic Laboratory (ADL) at McMaster University. Subsequently, reduced scale specimens with square dimensions of 70mm x 70mm were cut from this larger sheet. Each specimen comprised of 5 intermediate and 2 cover elastomer layers reinforced with a total of 6 bi-directional (orientations 0/90°) layers of carbon fiber fabric. The shape factor (*S*) and the aspect ratio (*AR*) of the specimens are given in **Table 1** along with the dimensions of the test specimens It is important to note that aspect ratio should be properly selected for U-FREI as it plays an important role in maintaining a stable lateral response throughout rollover deformation. It had been shown via experimental testing **[17]** and analytical modeling **[18]** that an aspect ratio larger than approximately 2.50 t_r (where t_r is the total thickness of the rubber) is required so that the U-FREI remains stable during lateral rollover (i.e. maintain a positive tangential stiffness).

This study was completed on reduced scale specimens, which ASCE [**19**], AASHTO [**6**] and several other standards accept as a means to evaluate the performance of full scale bearings. As such, experimental studies have been carried out on both full scale [**10, 20**] and reduced scale fiber reinforced elastomeric bearings [**17, 21-24**].

Table 1 – The geometric properties of the test specimens

Property	**Value**
Width (*a*)	70.00 mm
Length (2*b*)	70.00 mm
Total Bearing Height (*h*)	20.60 mm
Aspect Ratio (2*b* / *h*)	3.40
Shape Factor (*S*)	5.50

2.2 Three Dimensional (3D) Test Apparatus

The experimental testing program was carried out using a three-dimensional (3D) test apparatus designed specifically for testing seismic isolators under different load combinations. **Fig. 2** shows a photograph and schematic diagram of the test apparatus, which is capable of applying vertical loads, angles of rotations, and lateral displacements either independently or in combination on isolator specimens. The various load combinations are applied using the three actuators, two vertically oriented actuators located at either end of the loading beam, and one horizontal actuator that is connected to the end of the loading beam. The two vertical actuators apply the vertical loads and angles of rotation on the specimen, while lateral displacements are controlled using the lateral actuator. Triaxial load cells, located directly beneath the loading platen that supports the test specimen, were used to measure the vertical loads and shear forces on the specimen. The vertical deformations, which are typically small, were measured using high precision laser transducers. Finally, the lateral displacements were recorded using a string potentiometer attached at the center of the loading beam.

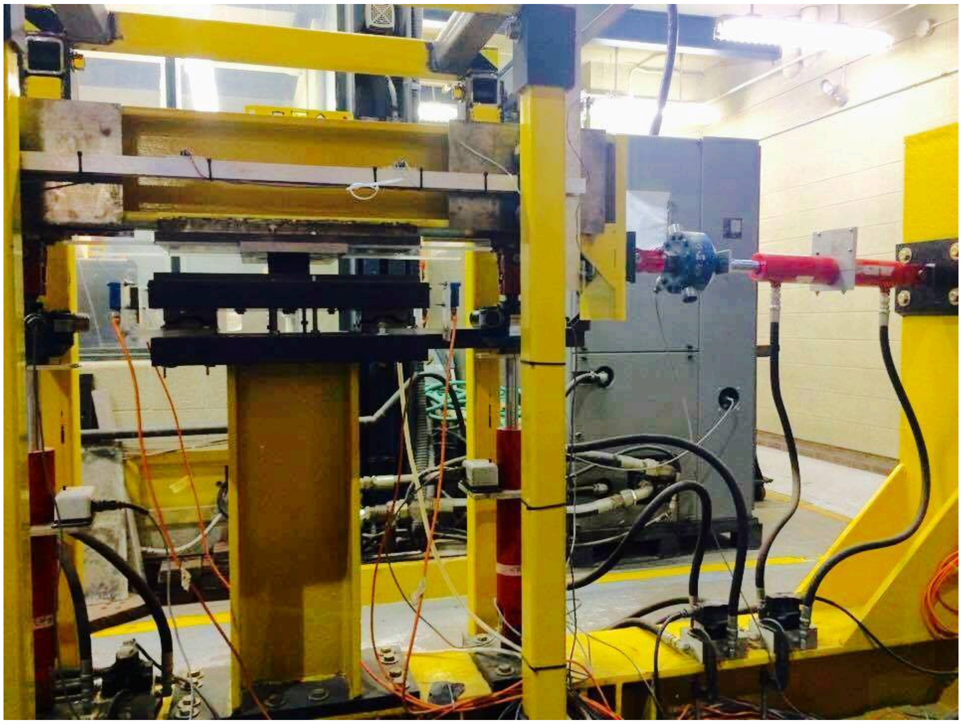

(a)

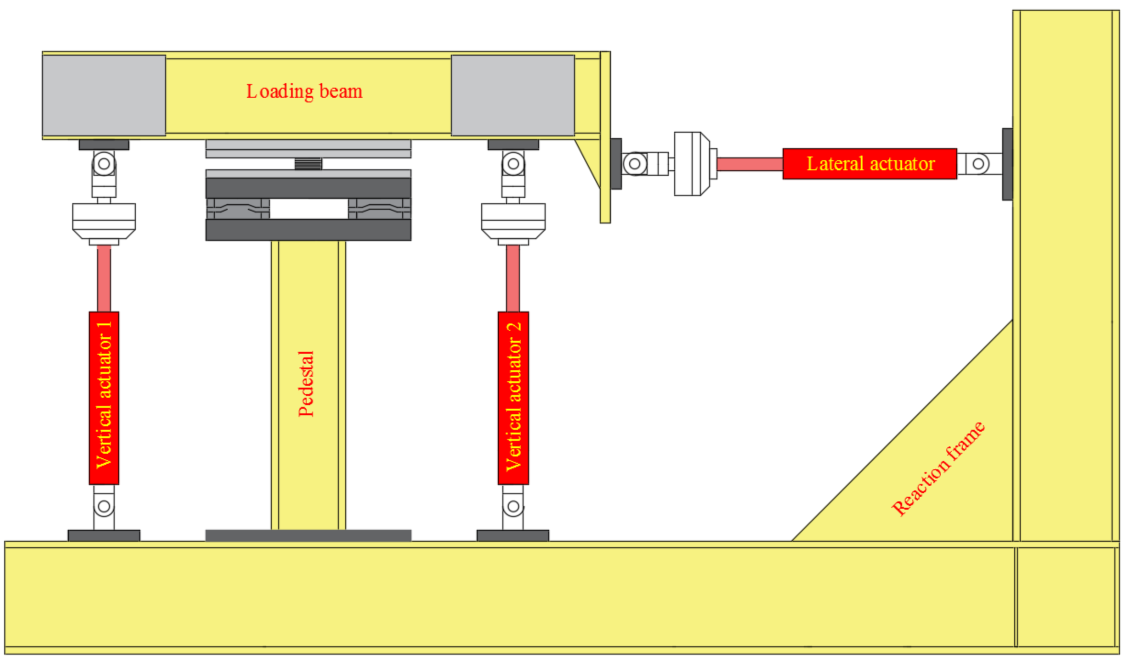

(b)

Fig. 2 – The employed 3D test-rig: (a) photograph; and (b) schematic

2.3 Experimental results

2.3.1 Influence of rotation on the vertical response of U-FREI

A series of vertical load tests were conducted on the U-FREI specimens in accordance with the procedures outlined in ISO-22762 **[25]**. In general, the U-FREI were subjected to five different levels of vertical load (*P*), which were expected to result in average vertical stress (σ_v) values of 2, 4, 6, 8, and 10 MPa under pure compression. First, the vertical load was applied monotonically on the specimen until it reached the target level of *P*. This was followed by the application of three full cycles of vertical load at an amplitude of ± 20% *P* at a loading rate of 0.2 Hz. Furthermore, the influence of static rotation, which represents a deformed bridge superstructure, was investigated by repeating the same aforementioned loading procedure, but under different levels of static rotation (θ) applied to the specimen after the application of the vertical load *P*, but prior to the application of the cyclic vertical load. Values of 0.01, 0.02, and 0.03 radians were considered for θ.

Fig. 3 presents the relationship between the vertical stiffness (K_v) and the vertical load (*P*) applied on the isolator for the considered static angles of rotations. K_v was determined using the peak values of vertical force (F_v) and displacement (Δ_v) observed over the vertical hysteresis loop corresponding to the third loading cycle as follows:

$$K_v = \frac{F_{v,max} - F_{v,min}}{\Delta_{v,max} - \Delta_{v,min}} \tag{1}$$

where $F_{v,max}$ and $F_{v,min}$ are the maximum and minimum forces and $\Delta_{v,max}$ and $\Delta_{v,min}$ are the corresponding maximum and minimum vertical displacements, respectively. **Fig. 3** shows that a nonlinear increase in the vertical stiffness occurs when the level of the applied vertical load is increased. Under low vertical load levels (i.e. < 2 MPa) a notable variation in vertical stiffness has been observed (defined as run-in **[20]**) due to the initial slackness in the fiber reinforcement layer if the fibers have not been pre-tensioned during construction. Under higher vertical loads the increase in vertical stiffness, in both steel and fiber reinforced, is affected by the elastomer material nonlinearity as well as the isolator geometric nonlinearity.

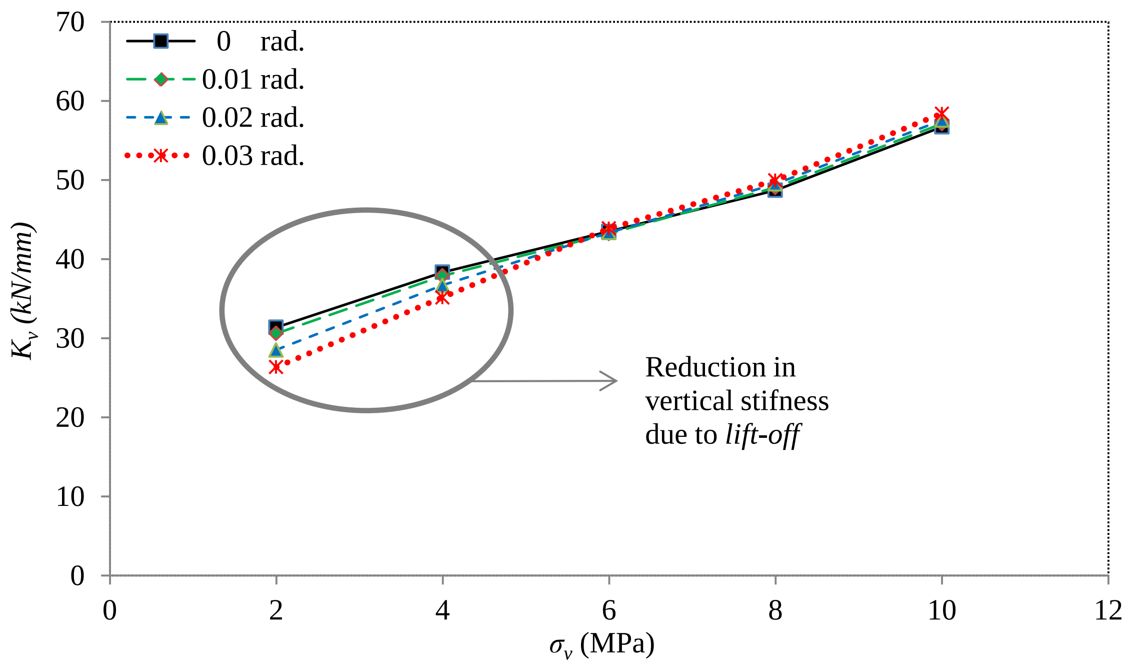

Fig. 3 – Influence of static rotation on the vertical response of U-FREI

It can also be observed from **Fig. 3** that the effect of static rotation on the vertical stiffness of the isolator is influenced by the occurrence of *lift-off*, which refers to the gap that develops between the U-FREI and the upper and lower support surfaces, resulting in a reduction in the loaded area of the isolator. Accordingly, an increase in the degree of *lift-off* is expected to lead to a reduction in the vertical stiffness of the isolator. However, it is important to note that the angle of rotation that initiates lift-off is dependent on the isolator aspect ratio and the level of applied vertical load. Thus, the occurrence of lift-off can be delayed/prevented for isolators having a higher aspect ratio (see **Fig. 4**) and under higher vertical load levels **[14-16]**. As such, it can be observed from **Fig. 3** that the effect of static rotation on the vertical response is reduced as the vertical load level is increased.

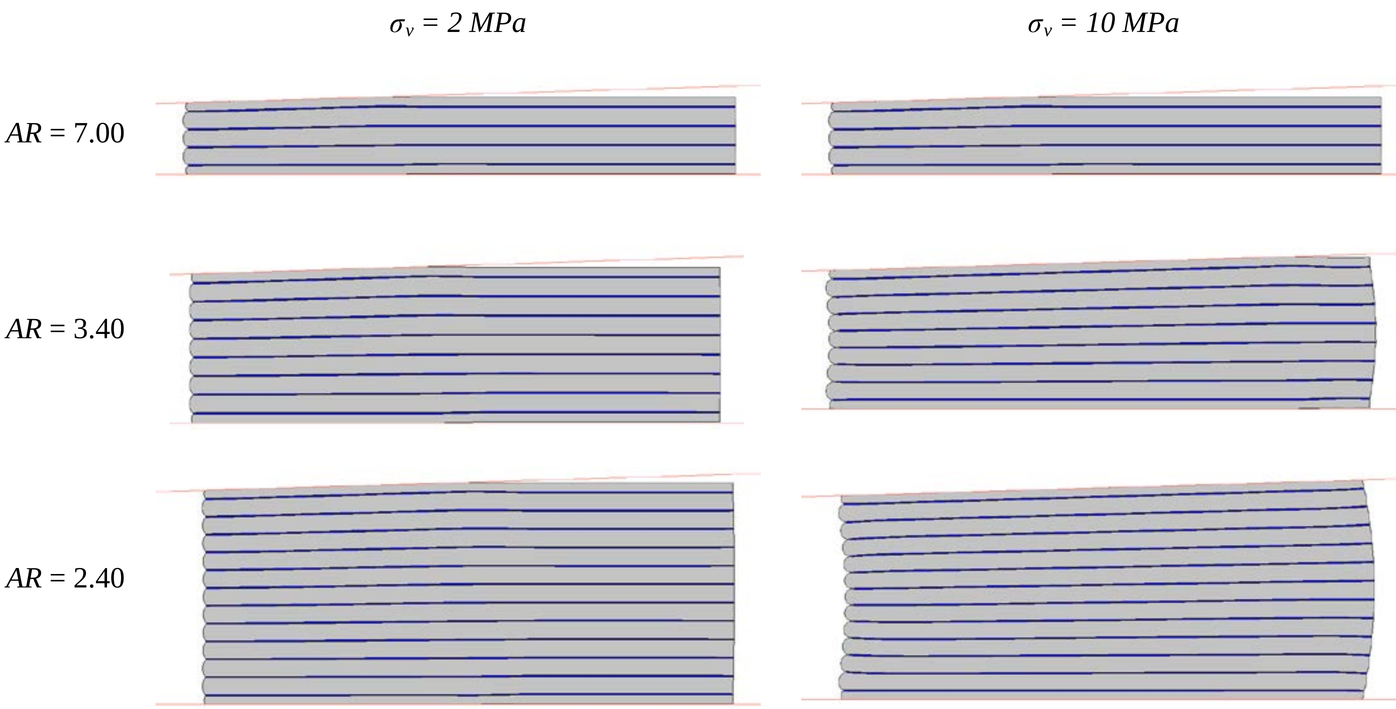

Fig. 4 – The lift-off development in U-FREIs with different aspect ratios at θ = 0.03 rad. and two different vertical stress ratios.

2.3.2 Influence of rotation on the lateral response of U-FREI

This subsection investigates the effect of static rotation on the lateral response of U-FREI. This was achieved through the application of cyclic lateral deformations at amplitudes of 0.25, 0.50, 1.00, 1.50, 2.00 t_r applied consecutively under displacement control at a lateral loading rate of 76 *mm/s*.

The lateral force-displacement behaviour of U-FREI under different levels of σ_v is presented in **Fig. 5a**. As shown, the force is normalized with respect to the plan area of the isolator (a), and the elastomer shear modulus (G), which was determined experimentally to be approximately 0.86 *MPa*. In general, the lateral response of U-FREI can be divided into three main stages as shown in **Fig.5b.** In the first stage, under small lateral displacements (i.e. < 0.5 t_r), the lateral force-displacement is nearly linear. The lateral response of U-FREI within this stage is consistent with that of bonded FREI as it remains in full contact with the upper and lower contact surfaces. Conversely, in the second stage, which occurs at higher lateral displacements (i.e. < approximately 1.67 h/t_r), the isolator exhibits nonlinear softening. The reduction in the lateral tangential stiffness is primarily due to the loss of contact area (i.e. shear area) between the isolator and the upper and lower supports as a result of the unbonded boundary conditions (i.e. geometric nonlinearity). However, at large lateral displacements (> approximately1.67 h/t_r), the U-FREI exhibits stiffening in the lateral response, which is the third stage of the response. This stiffening behaviour is due to the contact between the initial vertical surfaces of the isolator and the upper and lower supports.

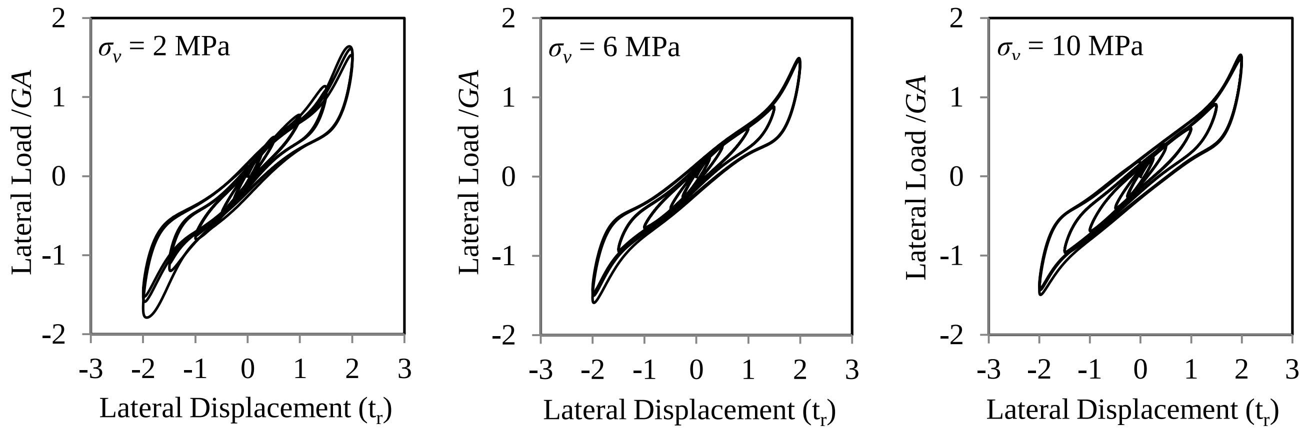

(a)

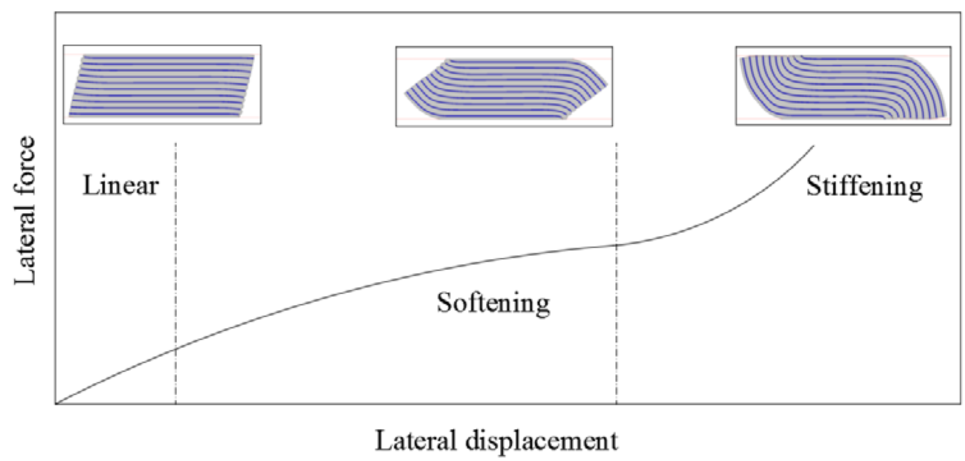

(b)

Fig. 5 – Typical relation between lateral force and lateral displacement for U-FREI

The same specimen was re-tested following the previous lateral loading protocol, but with the application of static rotation prior to being displaced laterally. The two lateral mechanical properties of interest to be compared are the effective lateral stiffness (K_L) and lateral damping (ζ_L). K_L was computed in a similar way as the vertical stiffness but using the peak lateral forces and lateral displacement (Δ_L) response values that were computed during each cycle. In addition, ζ_L was calculated using the area within the lateral hysteresis loop (W_D) using the following equation:

$$\zeta_L = \frac{2}{\pi}\left[\frac{W_D}{k_L(|\Delta_{L,max}| + |\Delta_{L,min}|)^2}\right] \tag{2}$$

It can be observed from **Fig. 6** that the influence of static rotation on the lateral response of U-FREI is negligible. However, a minor reduction in the lateral stiffness of the isolator is observed as well as an increase in the lateral damping with increased applied vertical load and/or applied angle of rotation. It is worth noting that a recent experimental study on U-FREI has shown that the vertical response is not significantly affected by the lateral rollover of the isolator **[26]**.

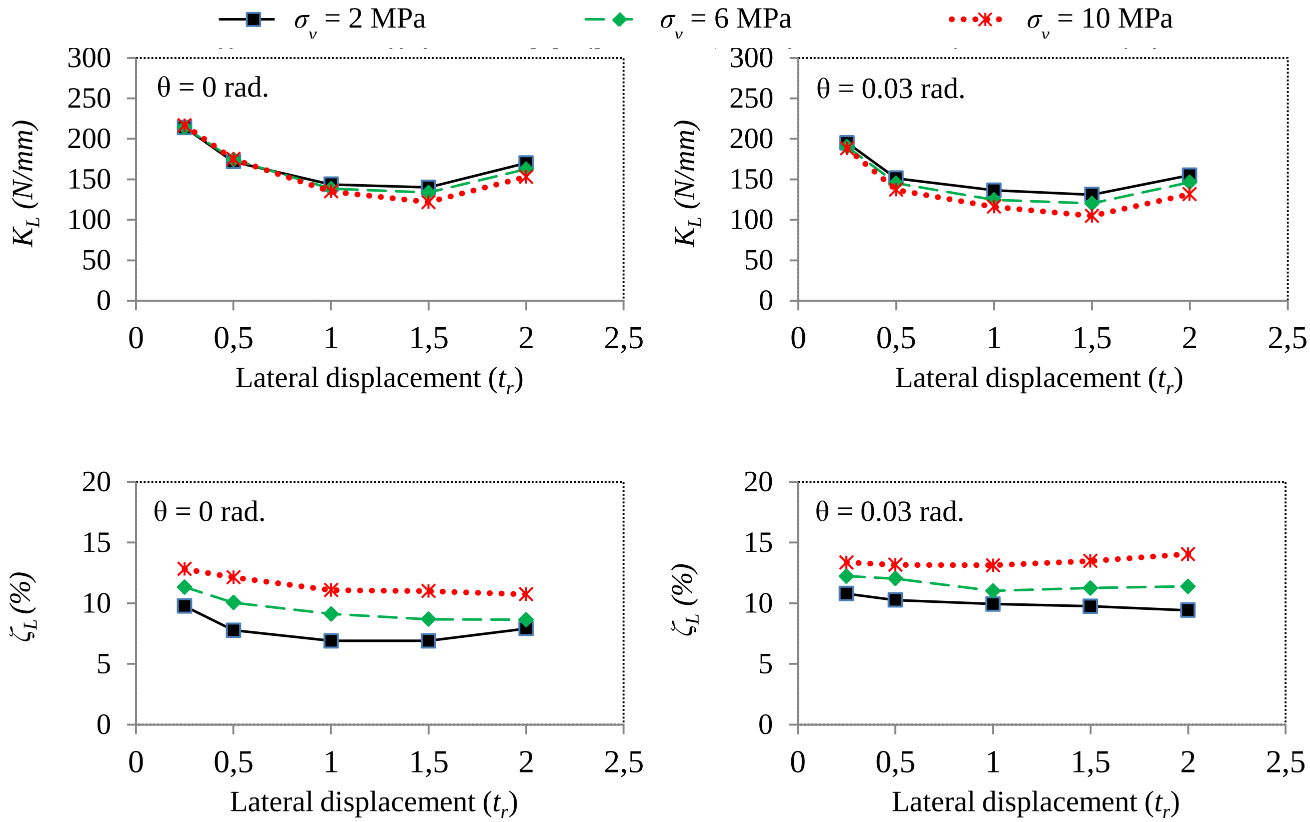

Fig. 6 – The influence of static rotation on the lateral stiffness and lateral damping of U-FREI (values obtained from the third lateral loading cycle)

3. Modelling of U-FREI

The objective of this section is to present simplified models that can be employed in order to simulate the lateral response of U-FREI. Typically, the lateral response of most seismic isolators (e.g. SREI) can be modelled with a bilinear model. The bilinear model is defined by three parameters, which are commonly defined as the initial stiffness K_1, the post-yield stiffness K_2, and the yield displacement U_y. However, as the lateral response of U-FREI exhibit both softening and hardening, this requires the value of K_2 to decrease under lateral displacements exceeding U_y until the initiation of contact between the vertical faces of the isolator and the upper and lower supports at which point the value of K_2 begins to increase. Additionally, the lateral damping of the isolator varies according to the lateral displacement amplitude. As such, a modified bilinear model, which requires an iterative approach to be employed, has successfully been used to model U-FREI **[27].** Three other iterative models that have been employed to represent the lateral response of U-FREI include a backbone curve model **[28]**, a 10-parameter rate-dependent multi-parameter model **[27]**, and a modified Bouc-Wen model **[29]**. As of the above models are iterative, the model parameters must be determined, typically using a least-squares regression analysis, from the hysteresis loops corresponding to each of the lateral displacement amplitudes.

More recently the lateral behavior of U-FREI has been simulated using non-iterative models (**Osgooei [27],** Van Engelen et al. **[31]** and Manzoori and Toopchi-Nezhad **[32])**. One attractive feature of the model proposed by Osgooei et al. **[30]** is that the parameters can be determined from the effective stiffness and damping values, avoiding the need to carry out fitting, for example using least squares, directly to the hysteresis loops. This model consists of two elements connected in parallel, one element to control the lateral stiffness value (e.g. Nonlinear elastic spring) and the other element to provide the required equivalent lateral damping at different lateral amplitudes (e.g. Pivot hysteresis **[30]**).

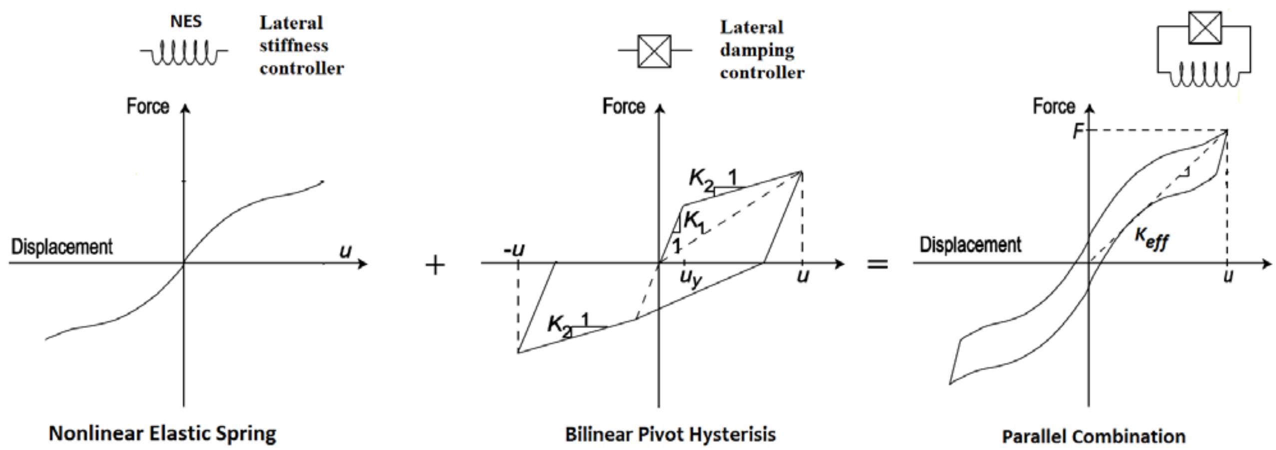

Fig. 7 – A parallel combination between a nonlinear elastic spring and a bilinear Pivot

As shown in **Fig. 7**, by assuming a parallel combination between a nonlinear spring with a 5th polynomial expression and a bilinear Pivot model, the effective lateral stiffness can be expressed as:

$$k_{eff} = [\ K_{spring}\ ] + [\ k_{Bilinear}\ ] + \ = [\ a_1 + a_2\, u^2 + a_3\, u^4\ ] + [\ k_1\ ] \qquad u < u_y$$

$$k_{eff} = [\ K_{spring}\ ] + [\ k_{Bilinear}\ ] \ = [\ a_1 + a_2\, u^2 + a_3\, u^4] + [\ (k_1 - k_2)\frac{u_y}{u} + k_2\ ] \qquad u \geq u_y \tag{3}$$

The effective damping (β_{eff}) is given at $u > u_y$ by:

$$\beta_{eff} = \frac{2}{4\pi}\left[\frac{(3k_1\, u_y\ +\ k_2\, u -\ k_2\, u_y).(k_1 -\ k_2).(u -\ u_y)}{k_{eff}\,.k_1.\ u^2}\right] \qquad \textit{Pivot hysteresis} \tag{4}$$

As previously mentioned, the above model parameters can be determined by minimizing the error between the values of the effective stiffness and effective damping ratio determined experimentally with those calculated from Eqs. (3) & (4). Table 2 presents the model parameters that were determined following the procedure described above. The model and experimental hysteresis loops, which are presented in Fig. 8, are found to be in reasonable agreement.

Table 2 – Parameters of the Pivot-Nonlinear Elastic Model

Parameter	**Value**
k_1 (N/mm)	307
k_2 (N/mm)	1.50
u_y (mm)	94.1
a_1 (N/mm)	49.9
a_3 (N/mm^3)	-0.066
a_5 (N/mm^5)	5.73E-05

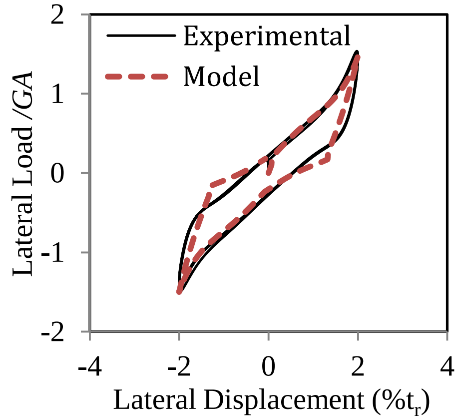

Fig. 8 – A Comparison between the Pivot-Nonlinear Elastic model and the experimentally determined lateral hysteresis loop under σ_V = 10 MPa

4. Conclusions

FREI utilize fiber fabric for the isolator reinforcement as an alternative to steel fibers and reinforcing plates. The introduction of flexible fiber reinforcement can improve the lateral performance of the isolator by allowing rollover as well as reducing the weight and manufacturing cost of the isolator. Research findings have shown that U-FREI possess acceptable vertical and lateral response characteristics that are suitable for building applications. However, extending the usage of U-FREI to bridge applications requires an understanding of the vertical and lateral response when coupled with rotational deformations.

This paper presents some of the findings of a larger experimental study performed on U-FREI to investigate their behaviour under different load/deformation scenarios typically expected during the lifetime of a bridge. The main finding of the study is that U-FREI are capable of resisting a range of vertical loads with and without the occurrence of rotational deformations. Furthermore, the lateral response of U-FREI was not significantly affected by the rotational deformation applied on the isolator. These findings further support the suitability of FREI as bridge bearings as well as seismic isolators.

In addition, this paper presents a simplified analytical model that can be used by bridge engineers to simulate the lateral response of U-FREI. This model is able to generate hysteresis loops representing the lateral behaviour of U-FREI based on lateral stiffness and damping values that have been determined experimentally.

5. Acknowledgements

This research was carried out as part of the mandate of the Centre for Effective Design of Structures (CEDS) at McMaster University and is partially funded by the Ontario Ministry of Economic Development and Innovation and by the Natural Sciences and Engineering Research Council of Canada (NSERC).

6. References

[1] Moustafa M, Mosalam K (2015). Seismic response of bent caps in as-built and retrofitted reinforced concrete box-girder bridges, *Engineering Structures*, 98: 59-73.

[2] Jangid R (2004). Seismic response of isolated bridges, *Journal of Bridge Engineering*, 9(2): 156–166.

[3] Constantinou M, Kalpakidis I, Filiatrault A, Ecker Lay R (2011). LRFD-based analysis and design procedures for bridge bearings and seismic isolators. *Report No. MCEER-11-0004*, Multidisciplinary Center for Earthquake Engineering Research, University at Buffalo, State University of New York, Buffalo, New York.

[4] Stanton J, Roeder C, Mackenzie-Helnwein P, White C, Kuester C, Craig B (2007). Rotation Limits for Elastomeric Bearings. *Report No. NCHRP 596*, Transportation Research Board, National Cooperative Highway Research Program, Washington, D.C.

[5] CSA. S6-14 (2014). Canadian Highway Bridge Design Code. Canadian Standards Association International, Ontario.

[6] AASHTO (2014a). AASHTO LRFD Bridge Design Specifications. 7th Ed., American Association of State Highway and Transportation Officials, Washington, D.C.

[7] AASHTO (2014b). Guide Specifications for Seismic Isolation Design. 4th Ed., American Association of State Highway and Transportation Officials, Washington, D.C.

[8] Kelly J, Takhirov S (2001). Analytical and Experimental Study of Fiber-Reinforced Elastomeric Isolators. *Technical Report PEER 2001/11*, Pacific Earthquake Engineering Research, Berkeley, USA.

[9] Kelly J (2002). Seismic isolation systems for developing countries, *Earthquake Spectra*, 18(3):385–406.

[10] Toopchi-Nezhad H, Tait M, Drysdale R (2008). Testing and modeling of square carbon fiber reinforced elastomeric seismic isolators, *Structure Control Health Monitoring*, 15(6): 876–900.

[11] Mordini A, Strauss A (2008). An innovative earthquake isolation system using fibre reinforced rubber bearings, *Engineering Structures*, 30(10): 2739–2751.

[12] Kelly J, Calabrese A (2012). Mechanics of fiber reinforced bearings. *Technical Report PEER 2012/101*, Pacific Earthquake Engineering Research, Berkeley, USA.

[13] Dezfuli F, Alam M (2013). Multi-criteria optimization and seismic performance assessment of carbon FRP-based elastomeric isolator, *Journal of Structural Engineering (ASCE)*, 49: 525:540.

[14] Al-Anany Y, Tait M (2015a). A Study on the Rotational Behaviour of Bonded and Unbonded Fiber Reinforced Elastomeric Isolators, *Proceedings of the 11th Canadian Conference on Earthquake Engineering*, Victoria, British Columbia, Canada, 21-24 July.

[15] Al-Anany Y, Tait M (2015b). A numerical study on the compressive and rotational behavior of fiber reinforced elastomeric isolators (FREI), *Composite Structures*, 133: 1249-1266.

[16] Al-Anany Y, Tait M (2016b). Experimental Assessment of Fiber Reinforced Elastomeric Isolators for Bridge Applications, *Composites part B: Engineering*, under review.

[17] Toopchi-Nezhad H, Drysdale R, Tait M (2009). Parametric study on the response of stable unbonded fiber-reinforced elastomeric isolators (SU-FREIs). *Journal of Composite Materials*, 43(15):1569–87.

[18] Van Engelen N, Tait, M, Konstantinidis D (2014). Model of the Shear Behavior of Unbonded Fiber-Reinforced Elastomeric Isolators, *Journal of Structural Engineering (ASCE)*, 141(7): 04014169.

[19] ASCE (2013). Minimum design loads for buildings and other structures. ASCE/SEI 7-10, New York.

[20] Kelly J (1999). Analysis of fiber-reinforced elastomeric isolators, *Journal of Seismology and Earthquake Engineering*, 2(1): 19–34.

[21] Warn G, Whittaker A (2006). A Study of the Coupled Horizontal-Vertical Behavior of Elastomeric and Lead-Rubber Seismic Isolation Bearings. Rept. No. MCEER-06-0011; Multidisciplinary Center for Earthquake Engineering Research, State University of New York at Buffalo.

[22] Toopchi-Nezhad H, Tait M, Drysdale R (2008). Lateral response evaluation of fiber-reinforced Neoprene seismic isolators utilized in an unbonded application, *Journal of Structural Engineering (ASCE)*;, 134(10):1627-1637.

[23] Love J., Tait M., Toopchi-Nezhad H. (2011). A hybrid structural control system using a tuned liquid damper to reduce the wind induced motion of a base isolated structure, *Engineering Structures*; 33(1): 738-746.

[24] Sanchez J, Masroor A, Mosqueda G, Ryan K (2013). Static and dynamic stability of elastomeric bearings for seismic protection of structures, *Journal of Structural Engineering (ASCE)*, 139(7): 1149–1159. [25] ISO. Elastomeric seismic-protection isolators. ISO 22762, Geneva, 2010.

[26] Al-Anany Y, Van Engelen N, Tait M (2016a). Experimental investigation on the vertical and lateral behaviour of unbonded fiber reinforced elastomeric isolators, Journal of Composites for Construction, under review.

[27] Toopchi-Nezhad H, Tait, M, Drysdale R (2009). Simplified analysis of a low-rise building seismically isolated with stable unbonded fiber reinforced elastomeric isolators, *Canadian Journal of Civil Engineering*, 36(7), 1182-1194.

[28] Toopchi-Nezhad H, Tait, M, Drysdale R (2007). Base isolation of small low-rise buildings using fiber reinforced elastomeric bearings, *CSCE 2007 Annual General Meeting & Conference.*

[29] Asl S. (2014). A Study of Integrated Structural Control Systems for Multi-Hazard Response Mitigation. M.A.Sc. thesis, McMaster University, Hamilton, Ontario.

[30] Osgooei P (2016). Advanced Numerical Modeling of Fiber-Reinforced Elastomeric Isolators (FREIs). Ph.D. thesis, McMaster University, Hamilton, Ontario.

[31] Van Engelen N, Konstantinidis D, Tait M (2015). Structural and nonstructural performance of a seismically isolated building using stable unbonded fiber reinforced elastomeric isolators, *Earthquake Engineering & Structural Dynamics*, 45(3), 421-439.

[32] Manzooria A, Toopchi-Nezhada H (2015). Application of an Extended Bouc-Wen Model in Seismic Response Prediction of Unbonded Fiber-Reinforced Isolators, *Journal of Earthquake Engineering*.